THE JOURNAL OF BIOLOGICAL CHEMISTRY
Vol. 277, No. 47, Issue of November 22, pp. 45529–45536, 2002
Printed in U.S.A.

Structural Analysis of the Autoinhibition of Ets-1 and Its Role in Protein Partnerships*

Received for publication, June 25, 2002, and in revised form, September 6, 2002
Published, JBC Papers in Press, September 6, 2002, DOI 10.1074/jbc.M206327200

Colin W. Garvie‡, Miles A. Pufall§, Barbara J. Graves§, and Cynthia Wolberger‡¶

From the ‡Department of Biophysics and Biophysical Chemistry and the Howard Hughes Medical Institute, Johns Hopkins University School of Medicine, Baltimore, Maryland 21205-2185 and the §Department of Oncological Sciences, Huntsman Cancer Institute, University of Utah, Salt Lake City, Utah 84112-5550

The DNA-binding activity of the eukaryotic transcription factor Ets-1 (E26 avian erythroblastosis virus oncogene-E twenty-six) is negatively regulated by inhibitory regions that flank the ETS domain. Based on the results of solution studies, these N- and C-terminal inhibitory regions have been proposed to pack against the ETS domain and form an autoinhibitory module whose N terminus partially unfolds upon binding of Ets-1 to DNA. Mutations that disrupt autoinhibition of DNA binding also cause a structural change in the inhibitory region. We report here a crystallographic study of fragments of Ets-1 that provide structural details of the inhibitory module and the structural transition that accompanies DNA binding. The structures of free and DNA-bound Ets-1 fragments containing the ETS domain and the inhibitory regions confirm that the N-terminal inhibitory region contains two α-helices one of which unfolds upon Ets-1 binding to DNA. The observations from the crystal structure, coupled with mutagenesis experiments, allow us to propose a model for the inhibited form of Ets-1 and lend insight into the flexible interaction between Ets-1 and the acute myeloid leukemia 1 protein, AML1 (RUNX1).

Transcription factors that bind to specific DNA sequences are essential in biological regulation. In addition to being controlled at the level of synthesis, transcription factors are regulated by a variety of mechanisms, including degradation (1), nuclear localization (2, 3), and post-translational modification (4). Autoinhibition is another commonly utilized mechanism for regulation of protein activity, including that of transcription factors. In this strategy a built-in negative control region inhibits the intrinsic functions of a protein. In the case of transcription factors, autoinhibitory domains have been shown to inhibit transcriptional activity, complex assembly, nuclear localization, or DNA binding. Autoinhibition can be enhanced or relieved through post-translational modification, proteolytic cleavage, or interaction with other proteins (5).

Autoinhibition of DNA-binding activity is observed among members of the ETS[1] family of eukaryotic transcription factors, including Elk-1, PEA3, and Ets-1 (6–12). Of these, Ets-1 is the best characterized. Ets proteins have in common a conserved 85-amino acid DNA-binding fold, termed the ETS domain, which belongs to the winged helix-turn-helix family (13, 14). Ets-1 is a 440-amino acid transcription factor that contains two regions that flank the ETS domain and inhibit DNA binding (Fig. 1). The DNA binding of full-length protein is recapitulated by a C-terminal fragment of Ets-1 comprising residues 280–440 (Ets-1ΔN280), indicating that the residues responsible for autoinhibition of Ets-1 reside within that fragment of the protein. Truncation of either the N-terminal inhibitory region (residues 280–330) or the C-terminal inhibitory region (residues 416–440) increases the DNA binding affinity of Ets-1 by 10- to 20-fold, indicating that the two inhibitory regions act in concert to impair DNA binding (15). Secondary structure determination of Ets-1ΔN280 by NMR spectroscopy indicates that the N-terminal inhibitory region contains two α-helices, HI-1 and HI-2 (16). The C-terminal inhibitory region contains a short α-helix, H4, followed by a longer helix, H5, as shown in the recent crystal structure of the uninhibited fragment of Ets-1, Ets-1ΔN331, bound to DNA (17). NMR chemical shift data suggest that the N- and C-terminal inhibitory helices pack against one another and against helix H1 of the ETS domain, forming an inhibitory module (16). When Ets-1 binds DNA, the first inhibitory helix, HI-1, appears to unfold, as assayed by protease sensitivity and circular dichroism spectroscopy (18). The energy required for this conformational change is proposed to contribute to the reduced affinity of full-length Ets-1 for DNA relative to Ets-1 fragments missing the N- or C-terminal inhibitory regions. However, the precise structural details of how the inhibitory regions interact when Ets-1 is free or bound to DNA are not known. Thus, the mechanism by which DNA binding is inhibited remains unclear.

To expand our understanding of the molecular details of Ets-1 autoinhibition and how the conformational switch is used for biological regulation, we have determined structures of free and DNA-bound Ets-1 protein fragments that contain N- and C-terminal inhibitory sequences. The structure of the inhibited fragment of Ets-1 (Ets-1ΔN280) bound to DNA was determined as part of a ternary complex with Pax-5, a paired domain protein that binds DNA cooperatively with Ets-1, and whose presence facilitated crystallization in complex with DNA. The

* This work was supported by the Howard Hughes Medical Institute (to C. W.), by the National Institutes of Health (Research Grant R01 GM38663 to B. J. G. and Fellowship Grants T32-CA93247 and T32-GM08537 to M. A. P.), and by the Huntsman Cancer Foundation. The costs of publication of this article were defrayed in part by the payment of page charges. This article must therefore be hereby marked "*advertisement*" in accordance with 18 U.S.C. Section 1734 solely to indicate this fact.

The atomic coordinates and structure factors (code 1MD0 and 1MDM) have been deposited in the Protein Data Bank, Research Collaboratory for Structural Bioinformatics, Rutgers University, New Brunswick, NJ (http://www.rcsb.org/).

¶ To whom correspondence should be addressed: Dept. of Biophysics and Biophysical Chemistry, Johns Hopkins University School of Medicine, 725 N. Wolfe St., Baltimore, MD 21205-2185. Tel.: 410-955-0728; Fax: 410-614-8648; E-mail: cwolberg@jhmi.edu.

[1] The abbreviations used are: ETS, E26 avian erythroblastosis virus oncogene-E twenty-six; DTT, dithiothreitol; MES, 4-morpholineethanesulfonic acid; r.m.s., root mean square; GABPα, GA-binding protein α; AML1, acute myeloid leukemia 1 protein.

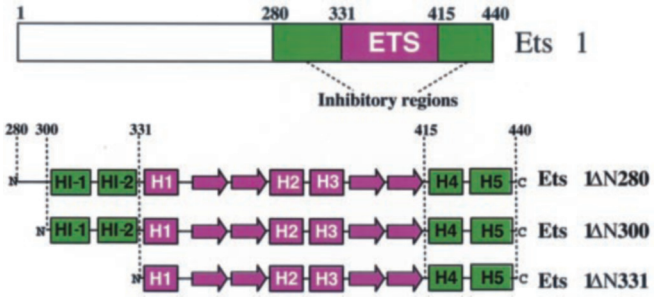

FIG. 1. **Domain structure of transcription factor Ets-1.** The secondary structure elements are indicated; α-helices are depicted by *rectangles* and β-strands as *arrows*. The secondary structure elements of the ETS domain are *purple*, and the N- and C-terminal inhibitory regions that flank the ETS domain are *green*.

structure of free Ets-1 was determined using a shorter fragment containing residues 300–440 (Ets-1ΔN300), which lacks the first 20 residues of the N-terminal inhibitory region that were predicted by NMR to be unstructured (16) (Fig. 1). The crystal structures confirm that Ets-1 has two N-terminal inhibitory helices, the first of which (HI-1) is disordered when Ets-1 is bound to DNA. In this form the inhibitory regions interact extensively with one another and with helix H1 of the ETS domain. In the absence of DNA, HI-1 contacts the N- and C-terminal inhibitory regions of a neighboring Ets-1 molecule in the crystal. The neighboring molecule participates in a reciprocal interaction, giving rise to what is known as a three-dimensional domain-swapped dimer (19). The intermolecular contacts made by HI-1 with the neighboring Ets-1 molecule suggest a model for intramolecular packing of the HI-1 helix that is supported by the results of mutagenesis experiments. The results of the structural and biochemical experiments described here provide new insights into the mechanism of autoinhibition and suggest how the inhibitory sequences may serve as interacting surfaces with DNA-binding partners of Ets-1.

EXPERIMENTAL PROCEDURES

Expression and Purification of Protein and DNA Used in Crystallographic Studies—The Ets-1ΔN280 (residues 280–440) and Ets-1ΔN300 (residues 300–440) fragments were expressed in *Escherichia coli* from plasmid pCWG2 and pCWG3, respectively, under control of a T7 promoter. BL21(DE3) cells were grown in LB medium at 37 °C and induced with 1 mM isopropyl-1-thio-β-D-galactopyranoside at mid-log phase for 1 h. The cells were resuspended in 500 mM NaCl, 5 mM DTT, 0.1% nonylphenol ethoxylate (IGEPAL), 1 mM EDTA, 100 mM Tris (pH 8.0) and lysed in a Microfluidizer (Microfluidics Corp.). The filtered lysate was dialyzed into 100 mM KCl, 5 mM DTT, 20 mM citrate buffer (pH 5.3), before loading onto an SP-Sepharose Fast Flow column (Amersham Biosciences) and eluting with a 0.1–1 M gradient of KCl. The peak fractions were pooled and dialyzed into 50 mM Tris (pH 8.0), 1 mM DTT, 50 mM NaCl and then loaded onto a Mono S column (Amersham Biosciences) and eluted with a gradient of 0.05–1.0 M NaCl. The peak fractions were concentrated and applied to a Superdex 75 column (Amersham Biosciences). The running buffer for the gel filtration column was 500 mM NaCl, 1 mM DTT, and 50 mM Tris (pH 8.0). The resultant peak fractions were collected and concentrated, and the protein was stored at −80 °C until needed. The Pax-5 (residues 1–149) fragment was expressed and purified as reported previously (17).

The oligonucleotides used for crystallization were synthesized by the phosphoramidite method on an Applied Biosystems DNA synthesizer and received with the trityl protecting group left on. Single-stranded oligonucleotides were purified by two successive runs over a Dynamax PureDNA column (Varian) with a 0–100% acetonitrile gradient in 0.1 M triethylamine acetate (pH 7). After the first purification, the trityl group was removed with 0.5% trifluoroacetic acid. The DNA was dialyzed against 10 mM triethylammonium bicarbonate at pH 7.0, lyophilized, resuspended in 10 mM triethylammonium bicarbonate at 20 mg/ml, annealed and then stored at −80 °C.

Crystallization—All crystallizations were carried out using the hanging drop vapor diffusion method with the drop consisting of 1 μl of complex solution and 1 μl of well solution. The Pax-5-(1–149)·Ets-1ΔN280·DNA complex was prepared for crystallization by mixing equimolar amounts of protein and DNA, followed by dialysis into 10 mM Tris (pH 8.0), 1 mM DTT. The ternary complex was crystallized using a duplex formed by annealing 5′-TTGCCGGAGATGGGCTCCAGTGGCCT-3′ and 5′-AAGGCCACTGGAGCCCATCTCCGGCA-3′, at a concentration of 0.32 mM. Fused crystals were obtained under well conditions of 200 mM ammonium acetate, 100 mM acetate buffer (pH 5.0), and 10% polyethylene glycol 4000. Data were collected on a fragment of a fused crystal. The complex crystallized in space group $P2_12_12_1$ with one molecule in the asymmetric unit and with unit cell dimensions a = 77.27 Å, b = 17.23 Å, and c = 44.71 Å.

TABLE I
Data collection and refinement statistics

Parameter	Ets-1ΔN280·Pax-5-(1–149)·DNA	Ets-1ΔN300
Resolution (Å)	35.0–2.8	50.0–2.0
Completeness (%) (outer shell)	87.8 (58.7)	94.4 (68.3)
Overall redundancy	3.1	3.4
Overall I/ (outer shell)	9.3 (4.0)	21.4 (4.9)
R_{sym} (%) (outer shell)	5.0 (19.2)	5.5 (17.6)
R_{cryst}/R_{free} (%)	25.9/31.0	20.9/23.6
r.m.s. bond length deviation (Å)	0.008	0.006
r.m.s. bond angle deviation (°)	1.36	1.12

The Ets-1ΔN300 fragment was crystallized at a concentration of 0.27 mM after dialysis into 50 mM NaCl, 10 mM Tris (pH 8.0). Single crystals grew with well conditions of 50 mM sodium citrate, 100 mM MES (pH 6.5), and 20% polyethylene glycol 4000. Ets-1ΔN300 crystallized in space group $P2_12_12_1$ with two molecules in the asymmetric unit and with unit cell parameters a = 53.35 Å, b = 66.67 Å, and c = 83.51 Å.

Structure Determination—All data were collected with the crystals frozen at liquid nitrogen temperature. The cryoprotectant consisted of the mother liquor plus 20% glycerol. Data were collected with an image plate detector (RAXIS IV) using CuKα radiation generated by a rotating anode Rigaku RU-200 generator. The datasets for the ternary complex and the Ets-1-(300–440) crystals were processed to 2.8 and 2.0 Å, respectively, using DENZO and SCALEPACK (Table I) (20). The structure factor amplitudes for each dataset were calculated with TRUNCATE (21).

The Pax-5-(1–149)·Ets-1ΔN280·DNA complex was solved by molecular replacement with AMoRe (21), using the previously reported crystal structure of the Pax-5-(1–149)·Ets-1ΔN331·DNA complex (17). After AMoRe, rigid body refinement was carried out followed by multiple cycles of simulated annealing, positional and grouped B-factor refinement in CNS (22), and model building in O (23) using $2F_o - F_c$ and $F_o - F_c$ maps. The final model had all the DNA, Pax-5 residues 19–142, and Ets-1 residues 309–437. The electron density for residues 310–318 of Ets-1 was very weak, and only the side chains for Arg-309 and Asp-310 could be clearly seen in the electron density maps. The remainder of the region from 311 to 318 was left as a polyalanine chain. The side chains for the region 88–141 of Pax-5 are included in the final model despite a lack of electron density to uniquely define their location. The poor definition of the amino acid side chains in this region of Pax-5 reflects the loss of contacts to the sugar-phosphate backbone, due to the less than optimal length of the DNA sequence used. Statistical details for the refined structures are summarized in Table I.

The initial phases for Ets-1ΔN300 were obtained using Ets-1ΔN280 from the ternary complex as a search model in AMoRe. Refinement was carried out as for the ternary complex, except the higher resolution allowed individual *B*-factors to be refined and the addition of water molecules. The final refined model for the Ets-1Δ300 fragment consists of residues 300–437 for both protein fragments in the asymmetric unit and a total of 271 water molecules. Statistical details for the refined structures are summarized in Table I.

Site-directed Mutagenesis and Construction of Bacterial Expression Constructs—Mutagenesis was performed using a QuikChange™ site-directed mutagenesis kit (Stratagene) in Ets-1ΔN280 or Ets-1ΔN331 as described previously (18). The L422A and Y424A mutants were made in both Ets-1ΔN280 and Ets-1ΔN331, whereas the F304A and Y307A mutants were made in Ets-1ΔN280 only. The primers used to generate the mutations are as follows (top strand only shown): F304A, 5′-G CCC AAG GGC ACC GCC AAG GAC TAT GTG-3′; Y307A, 5′-GGC ACC TTC AAG GAC GCT GTG CGT GAC CGT GC-3′; L422A, 5′-GAC CTG CAG AGC CTG GCG GGA TAC ACC CCT GAA-3′; Y424A, 5′-CAG AGC CTG GGA GCC ACC CCT GAA GAG CTG-3′.

Protein Expression and Purification for Mutagenesis Studies—All versions of Ets-1ΔN280 and Ets-1ΔN331 for mutagenesis study were

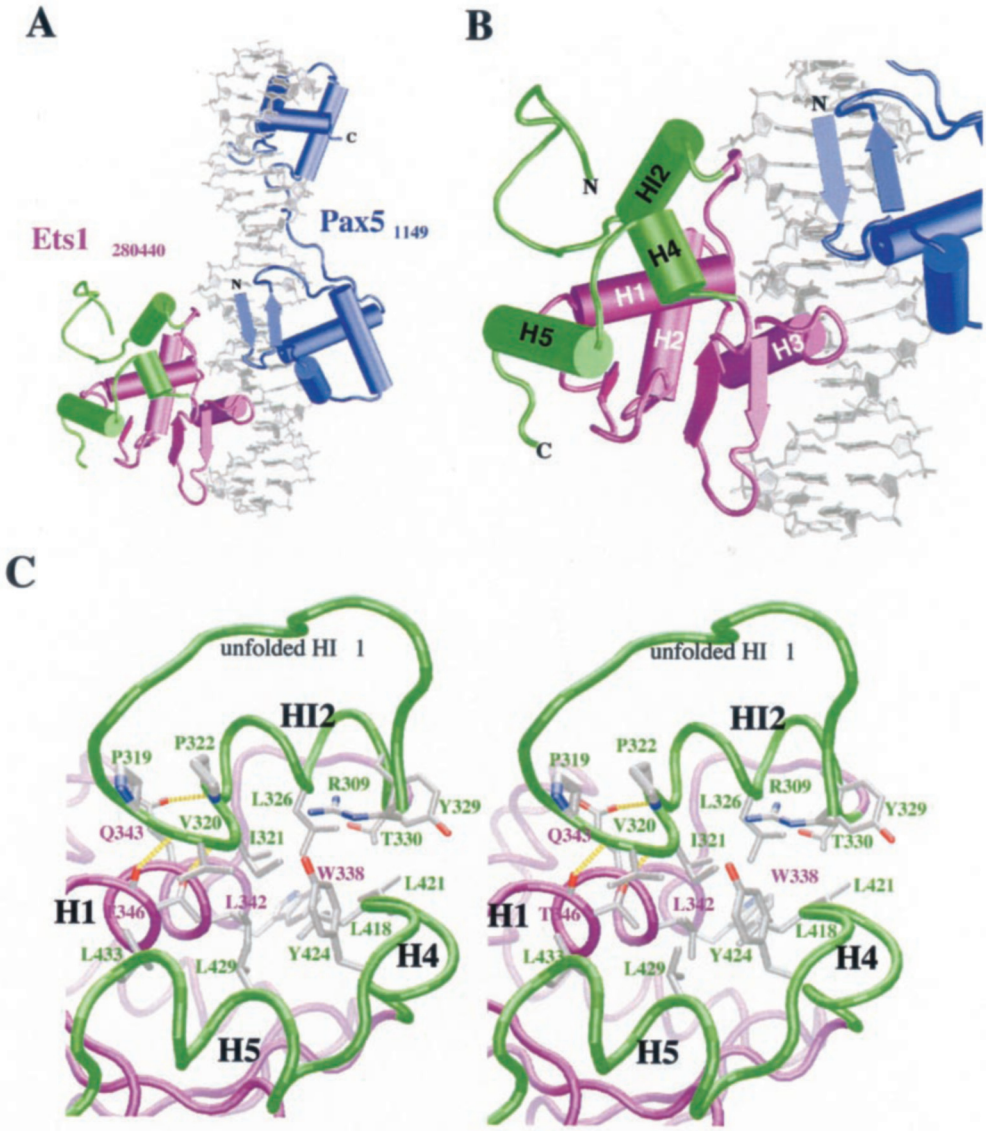

FIG. 2. **Crystal structure of Ets-1ΔN280 bound to DNA.** *A*, overview of Ets-1ΔN280 and Pax-5-(1–149) bound to DNA. The paired domain of Pax-5 is represented in *blue*, the ETS domain of Ets-1 in *magenta*, and the inhibitory regions of Ets-1 in *green*. *B*, enlarged view of Ets-1ΔN280 in the ternary complex. *C*, stereoview of the interactions made by the N- and C-terminal inhibitory regions with each other and the ETS domain of Ets-1. The residues are *green* and *magenta* depending on whether they come from the inhibitory regions or ETS domain, respectively.

expressed and purified as previously described for both wild type and mutant versions of these proteins (24). Briefly, proteins were expressed in BL21(DE3) *E. coli* and lysed by sonication, and soluble species were purified by conventional cation exchange followed by gel filtration chromatography. Purity was subsequently estimated to be greater than 90% by Coomassie staining of SDS-PAGE gels. Concentration was determined spectrophotometrically by denaturing the protein with guanidine hydrochloride and calculating the extinction coefficient based on amino acid composition.

Proteolysis Assays—Partial proteolysis assays on the Ets-1Δ280 mutants were performed by incubating 2 μg of wild type or mutant protein with 0, 0.1, 0.2, and 2 μg of trypsin (Sigma, T8642), in 25 mM Tris, pH 8.0, 10 mM $CaCl_2$. The reaction mixtures were stopped after 3 min by adding SDS running buffer, boiling for 5 min, running on 18% SDS-polyacrylamide gels, and visualized by staining with Coomassie Blue.

DNA Binding Assays—The 9-bp high affinity binding site, termed SC1 (25), was used as the Ets-1 recognition site in all assays. The oligonucleotides for this binding site are as follows: 5′-GCCAAGCCGGAAGTGTGTGGTAAGCAG-3′ (top strand, SC1–27); 5′-CTGCTTACCACACACTTCCGGCTTGGC-3′ (bottom strand, SC1–27). DNA binding assays were performed and quantified as previously described (13). In brief, both strands of the DNA duplexes were 5′-end-labeled with T4 polynucleotide kinase and [γ-^{32}P]ATP (4500 Ci/mol) and annealed (15). DNA and protein dilutions were mixed, allowed to reach equilibrium with 30-min incubation, then loaded on running native gels. Radioactivity was detected by phosphorimaging. Equilibrium dissociation constants (K_D) were measured by plotting free protein concentration [*P*] *versus* fraction of DNA bound ([*PD*]/*Dt*) and curve fitting to [*PD*]/*Dt* = 1/(1 + (K_D/[*P*])) (15). Data points are mean values from three experiments. Error bars represent standard deviation of the mean for each point.

RESULTS

Structure of Inhibited Ets-1 Bound to DNA with Pax-5—The structure of the inhibited Ets-1 fragment bound to DNA was obtained by co-crystallizing Ets-1ΔN280 (residues 280–440) as part of a ternary complex with both DNA and the paired domain of Pax-5 (Fig. 2*A*). Pax-5 was included to facilitate crystallization, because a Pax-5·Ets-1·DNA complex containing a shorter fragment of Ets-1 (residues 331–440) and lacking the N-terminal inhibitory sequences had been shown to crystallize readily (17). As expected, the interaction between Pax-5 and Ets-1 on DNA occurs solely through contacts made between the paired domain of Pax-5 and the ETS domain of Ets-1 and does not involve the inhibitory regions of Ets-1 (17). As compared with previous crystal structures of Ets-1 bound to DNA (17), the Ets-1 protein fragment used in the present structure con-

tains an additional 51 amino acids at the N terminus (residues 280–330). The crystal structure of Ets-1ΔN280 and the Paired domain of Pax-5 bound to a 24-bp DNA duplex was determined at a resolution of 2.8 Å. The final refined model for the complex contains all 24 bp of the DNA, Ets-1 residues 309–436, and Pax-5 residues 19–142. With the exception of the additional N-terminal residues in Ets-1, the structure of the Ets-1ΔN280·Pax-5·DNA complex (Fig. 2*A*) is essentially identical to that of the previously determined Ets-1ΔN331·Pax-5·DNA complex (17). The two complexes superimpose with a root mean square (r.m.s.) deviation of 0.61 Å for all common protein main-chain atoms and an r.m.s. deviation of 0.82 Å for all common DNA atoms. The conformation of the minimal ETS domain of Ets-1 (residues 331–415) is identical to that observed in previous crystal structures of Ets-1. Briefly, the ETS domain is composed of three α-helices (H1, H2, and H3) and a four-stranded, anti-parallel β-sheet. The ETS domain makes base specific DNA contacts by inserting helix H3 into the major groove (Fig. 2, *A* and *B*). Because the details of the ETS domain and the Pax-5·Ets-1 interaction are identical to those observed in the Ets-1ΔN331·Pax-5·DNA complex, we focus our discussion on the additional inhibitory sequences in Ets-1ΔN280 and their packing against the ETS domain (Fig. 2*C*).

The crystal structure of Ets-1ΔN280 bound to DNA displays the disrupted conformation of the Ets-1 inhibitory module. The additional N-terminal residues contain a single α helix (residues 323–329) located immediately N-terminal to the ETS domain corresponding to helix HI-2 (Fig. 2*B*). The first 29 residues of the DNA-bound Ets-1ΔN280 protein, residues 280–308, are disordered. The first ordered residue in the N-terminal inhibitory region is Arg-309, which is stabilized by the packing of the arginine side-chain atoms in a hydrophobic pocket created by Ile-321 in the loop preceding HI-2, Leu-326 and Tyr-329 from HI-2, and Tyr-424 from the C-terminal inhibitory region (Fig. 2*C*). The following nine residues (310–318) have poorly defined electron density, indicating that this region is relatively unstructured. The remainder of the N-terminal inhibitory region comprises a loop region (319–322) and an α-helix (323–329) that corresponds to HI-2 predicted by NMR secondary structure determination (16). The C-terminal inhibitory region contains two α-helices, H4 (418–422) and H5 (426–433), that pack on the face of the ETS domain that is opposite to the DNA binding surface (Fig. 2*B*). These C-terminal residues adopt the same conformation seen in previous crystal structures of Ets-1 bound to DNA, which contained the C-terminal, but not the N-terminal, inhibitory region (17). The conformation of the Ets-1 residues C-terminal to the ETS domain is also similar to that observed in GABPα (26), which contains a similar C-terminal sequence. GABPα lacks homologous N-terminal inhibitory residues and does not exhibit autoinhibition.[2]

The structure of Ets-1ΔN280 in complex with DNA reveals how the N-terminal inhibitory region interacts with the ETS domain and the C-terminal inhibitory region in the bound state (Fig. 2*C*). A well-packed hydrophobic interface, along with a number of hydrogen bond contacts, stabilizes the packing of the ordered N-terminal inhibitory region against the C-terminal inhibitory domain and helix H1 of the ETS domain (Fig. 2*C*). The loop preceding helix HI-2 is stabilized in part by van der Waals packing of Pro-319 against Pro-322, in addition to two hydrogen bonds between the main-chain nitrogen atoms of Val-320 and Ile-321 and ETS domain helix H1 residues Thr-346 and Glu-343, respectively (Fig. 2*C*). The side chains of loop residues Val-320 and Ile-321 also make extensive hydrophobic contacts with side chains from the ETS domain and the C-terminal inhibitory region: Val-320 makes van der Waals contacts with Thr-346 of helix H1 of the ETS domain, Tyr-424 of the loop between H4 and H5 of the C-terminal domain, and Leu-429, Met-432, and Leu-433 of H5. Ile-321 forms van der Waals contacts with Leu-326 of inhibitory helix, HI-2, and Leu-422 in the C-terminal inhibitory helix, H4. Additional contacts are mediated by Tyr-329 and Thr-330 of HI-2 with Leu-421 of H4. The N-terminal inhibitory domain helix HI-2 also contacts helix H1 of the ETS domain with a hydrogen bond between the main chain nitrogen of Ala-323 and Glu-343 of helix H1 as well as van der Waals contact between Leu-326 of HI-2 and Trp-338 of H1 (Fig. 2*C*).

Ets-1 Contains an Additional N-terminal Helix in the Absence of DNA—The structure of the uncomplexed Ets-1 protein was determined at 2.0-Å resolution using the fragment Ets-1ΔN300, containing residues 300–440. The deletion of the region comprising residues 280–299, which is predicted to be unstructured by NMR (16), was necessary to obtain crystals of the free protein. Ets-1ΔN300 crystallized with two molecules in the asymmetric unit, with each molecule related to the other by a non-crystallographic 2-fold symmetry axis. The two Ets-1ΔN300 molecules are essentially identical in structure and only one will be discussed here in detail, except where necessary.

The crystal structure of Ets-1ΔN300 confirms the presence of a second N-terminal inhibitory helix when Ets-1 is not bound to DNA (Fig. 3*A*). The first 18 residues (residues 300–317) are fully ordered in the Ets-1ΔN300 structure. These ordered residues contain an additional α-helix (residues 303–313) corresponding to helix HI-1 that was identified initially by NMR (16). Helix HI-1 is flanked on either side by two ordered loop regions, comprising residues 300–302 and residues 314–317, that do not contact the ETS domain or inhibitory regions. The remainder of Ets-1ΔN300, residues 318–440, is essentially identical to the related region in the Ets-1ΔN280·Pax-5·DNA complex, with an r.m.s. deviation for the protein main-chain atoms of 0.68 Å.

Unexpectedly, Ets-1ΔN300 forms a dimer in the asymmetric unit. Specifically, helix HI-1 packs against a second Ets-1ΔN300 molecule rather than forming predicted intramolecular contacts (Fig. 3, *B* and *C*). There are reciprocal interactions between the two proteins in the asymmetric unit. Each Ets-1ΔN300 molecule contacts the other by inserting helix HI-1 side chain, Phe-304, of one molecule, into a hydrophobic pocket that is formed by residues from the N- and C-terminal inhibitory regions of the opposing monomer (Fig. 3*C*). The hydrophobic pocket is composed of side chains Ile-321 from the loop preceding helix HI-2, Leu-326 and Tyr-329 of HI-2, Leu-422 of H4, and Tyr-424 of the loop between H4 and H5. Tyr-307 from helix HI-1 also contributes to the interface between Ets-1ΔN300 molecules by forming van der Waals interactions with Tyr-329.

Modeling of the Inhibited Form of Ets-1Δ280 and Mutational Studies—The crystal structure of the free Ets-1ΔN300 dimer provides clues to the packing of helix HI-1 in the inhibited molecule. The intermolecular interactions within the dimer formed by Ets-1ΔN300 (Fig. 3*B*) are likely due to crystal packing, because Ets-1 does not dimerize in solution, even at millimolar concentrations.[3] Instead, extensive biochemical data suggest that HI-1 forms part of an inhibitory module that connects to the ETS domain by intramolecular interactions (6). The metastability of HI-1, evidenced by its unfolding upon DNA binding, suggests that it may be a loosely associated

[2] A. H. Batchelor and C. Wolberger, unpublished results.

[3] C. W. Garvie and C. Wolberger, unpublished results.

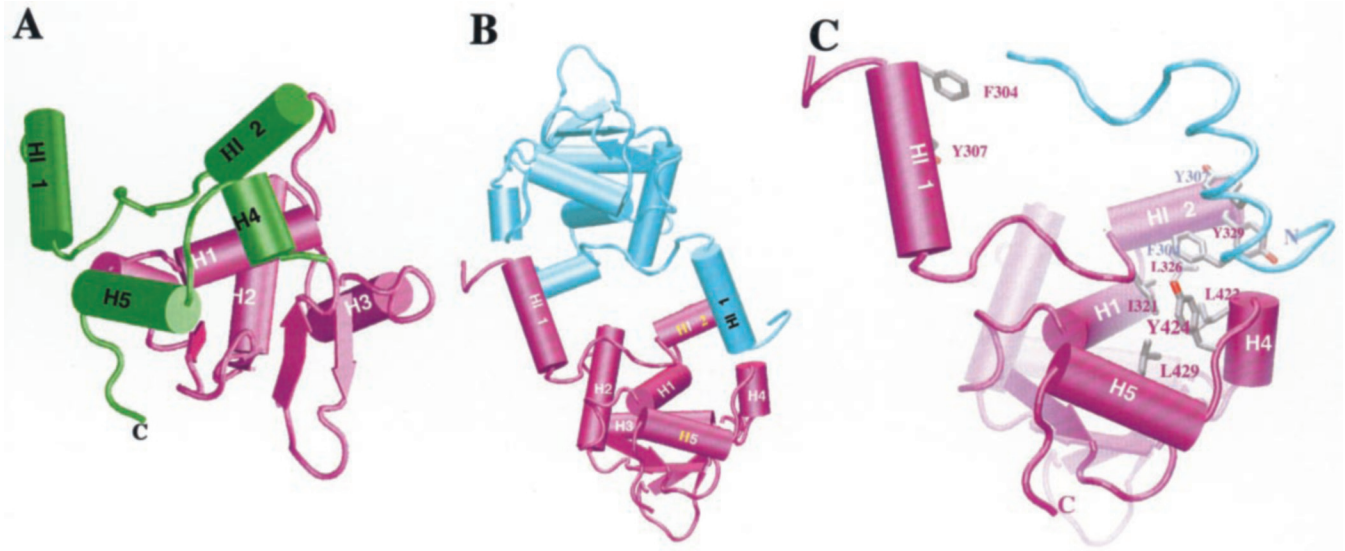

FIG. 3. **Crystal structure of Ets-1ΔN300.** *A*, Ets-1ΔN300 molecule. The ETS domain is represented in *magenta*, whereas the inhibitory regions are represented in *green*. *B*, three-dimensional domain-swap dimer formed by one molecule of Ets-1ΔN300 (*cyan*) with the other Ets-1ΔN300 molecule (*magenta*) in the asymmetric unit. *C*, crystal packing contacts made by helix HI-1 from one Ets-1ΔN300 molecule (*cyan*) with the other Ets-1ΔN300 molecule (*magenta*) in the asymmetric unit. The residues involved in this interaction are labeled with a color denoting whether they come from the HI-1 helix of one Ets-1ΔN300 molecule (*cyan*) or from the hydrophobic pocket of the second Ets-1ΔN300 molecule (*magenta*).

component of the autoinhibitory domain. We therefore hypothesize that this loosely tethered helix associates with a neighboring molecule in the crystal to form a three-dimensional domain-swapped dimer (19) in which the interaction of HI-1 with the remainder of the Ets-1 protein approximates the intramolecular contacts that would form in an inhibited Ets-1 monomer. In the proposed monomer, the N terminus of HI-1 would be in close proximity to the C-terminal end of H4 of the inhibitory module, as observed in the crystallographic dimer (Fig. 3*C*). This orientation of helix HI-1 would allow hydrophobic residues at the N terminus of HI-1, such as Phe-304 and Tyr-307, to form van der Waals contacts with residues from HI-2 of the N-terminal inhibitory region and Leu-422 and Tyr-424 from the C-terminal inhibitory region (Fig. 4). Previous NMR data showed large chemical shift differences in residues Leu-422 and Tyr-424 on comparison of unbound Ets-1ΔN331 and unbound Ets-1ΔN280 (16). The change in chemical shifts of these two residues suggests that these C-terminal residues are in direct contact with the N-terminal inhibitory region, which supports our proposed model.

To test the validity of the model for the monomeric inhibited Ets-1, we investigated the effects on DNA binding of alanine substitutions of Phe-304, Tyr-307, Leu-422, and Tyr-424, in the Ets-1 fragments Ets-1ΔN280 and Ets-1ΔN331. Autoinhibition is characterized by the ratio of equilibrium dissociation constants of Ets-1ΔN280 and Ets-1ΔN331, shown here to be ~16-fold (Fig. 5*A*). The H4/H5 mutations, L422A and Y424A, had a minimal effect on the DNA-binding activity of an ETS domain fragment, Ets-1ΔN331, indicating that these mutations do not result in structural changes in the ETS domain that affect DNA binding. Ets-1ΔN280 and Ets-1ΔN331 with mutation Y424A showed almost identical affinity, suggesting a dramatic disruption of autoinhibition. Similarly, mutation of Phe-304 and Tyr-307 in helix HI-1 retained only 3-fold inhibition. Interestingly, mutation of Leu-422 to alanine had little effect on the differential binding affinity between Ets-1ΔN280 and Ets-1ΔN331, suggesting retention of autoinhibition and a lesser role for Leu-422 in stabilizing contacts with HI-1.

The mutagenesis data are consistent with residues Phe-304, Tyr-307, and Tyr-424 being part of the intramolecular interface between the autoinhibitory module and the ETS domain. The

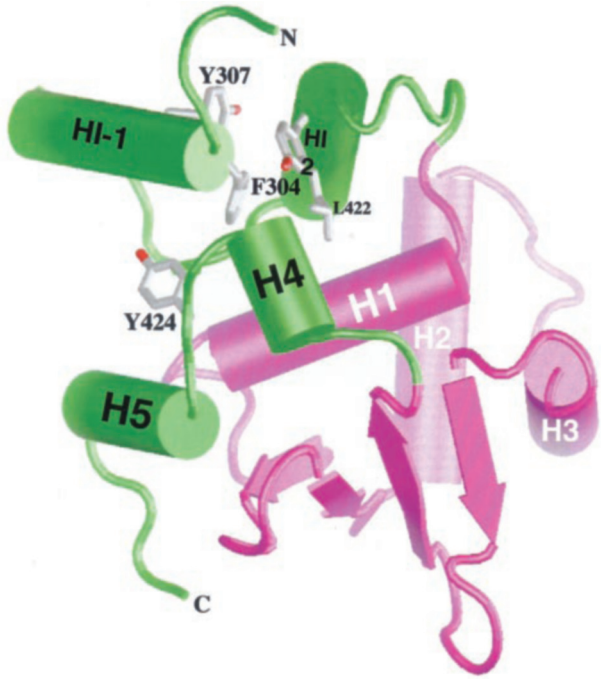

FIG. 4. **Model of the inhibited form of Ets-1.** The four residues that were individually mutated to alanine to test the effect on autoinhibition of Ets-1ΔN280 are indicated. Other residues that may contribute to the hydrophobic interaction between helix HI-1 and the N- and C-terminal inhibitory regions are also shown, but not labeled.

activated DNA binding of the Ets-1ΔN280 fragments containing these mutants suggest that this interface has been disrupted, leaving an inhibitory module that is no longer functionally coupled to DNA binding. This model predicts that these mutations would cause the inhibitory module to be constitutively disrupted. Previous partial proteolysis studies had established that a conformational change accompanies DNA binding. A 16-kDa tryptic fragment is generated due to cleavage immediately C-terminal to helix HI-1 in the presence, but not absence, of DNA (Fig. 5*B*). The enhanced sensitivity of this site in the presence of DNA correlates with the loss of helicity

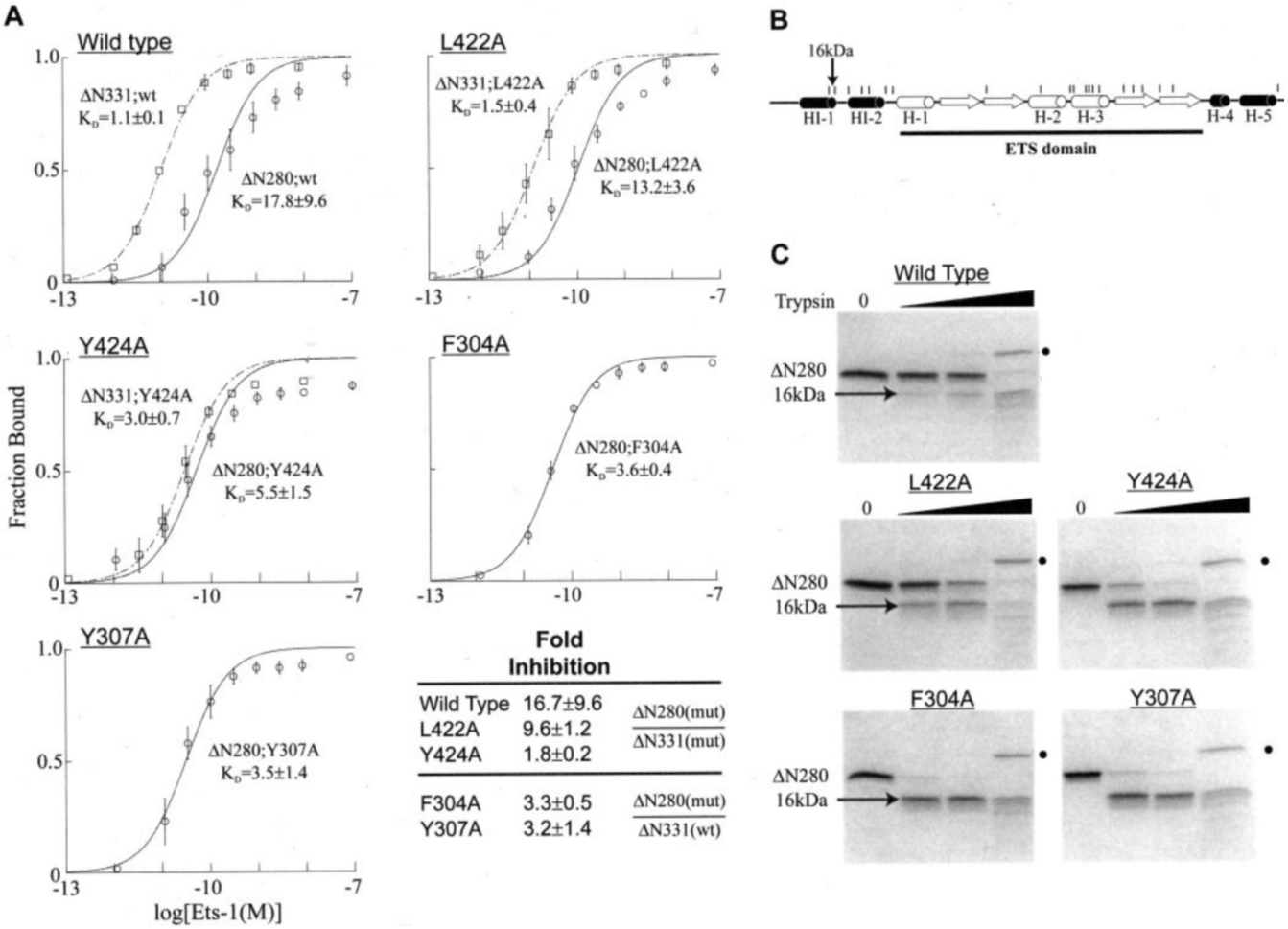

FIG. 5. **Disruption of inhibitory module correlates with reduction in autoinhibition.** *A*, equilibrium DNA binding curves derived from electrophoretic mobility shifts of mutants made in Ets-1ΔN280 (inhibited) and Ets-1ΔN331 (activated). *Dashed* and *solid lines* indicate data from Ets-1ΔN331 and Ets-1ΔN assays, respectively. Data are from three independent experiments. K_D values are to be multiplied by 10^{-11} and are in units of molarity. The fold inhibition was calculated as the K_D of the Ets-1ΔN280 species divided by the K_D of the Ets-1ΔN331 species for the wild type and mutants, where possible (L422A and Y424A). The -fold inhibition of the F304A and Y307A mutants was calculated as the K_D of the Ets-1ΔN280 mutant species divided by the K_D of the wild type Ets-1ΔN331 species. *B*, schematic secondary structure diagram of Ets-1ΔN280. *Vertical lines* mark potential trypsin digestion sites. Conformation of the autoinhibitory module is assayed by trypsin sensitivity at residues 310 and 312 that probes the folded state of helix HI-1. *C*, partial proteolysis of the wild type and mutant versions of Ets-1ΔN280 separated by 18% SDS-PAGE and stained with Coomassie Blue. The 16-kDa band represents cleavage at position of helix HI-1 (see *B*). ●, trypsin band.

in Ets-1ΔN280 (18). Importantly, mutations in the Ets-1ΔN280-inhibited fragment that enhance DNA binding, including L429A and Q339E, result in enhanced protease sensitivity in the absence of DNA (24). Enhanced trypsin cleavage was observed in the activated mutants, F304A, Y307A, and Y424A, indicating constitutive unfolding of HI-1 (Fig. 5*C*). Consistent with DNA binding data, the effect of the L422A mutation on the conformation of the inhibitory module was modest. The activated DNA binding and protease sensitivity of mutants F304A, Y307A, and Y424A are consistent with these residues being involved in packing at the intramolecular interface. We conclude that, in the Ets-1ΔN300 monomer, HI-1 packs against the remainder of the Ets-1 fragment. Specifically, residues from the N terminus of HI-1 form a hydrophobic network with residues from the N- and C-terminal inhibitory regions (Fig. 4). The extensive interactions between Leu-422 and residues in HI-1 and HI-2 indicated by the domain-swapped crystal structure suggest that this leucine has a similar role in maintaining stability of the autoinhibitory module. However, the less severe phenotypes of the L422A mutant do not support a major role. Thus, the orientation of HI-1 at the interface in the monomer could be slightly different from that observed in the dimer.

DISCUSSION

Structure of the Inhibitory Module of Ets-1—This report provides the first high resolution structural view of the inhibitory components of Ets-1 and gives new insight into the possible three-dimensional packing of the autoinhibitory module. Previous studies had identified the presence of N- and C-terminal inhibitory sequences flanking the ETS domain (16) and showed that inhibition of DNA binding depended upon a structural coupling between the two inhibitory regions and the ETS domain itself (5). The crystal structures described in the present study show how the inhibitory elements are positioned in two different fragments of Ets-1: Ets-1ΔN280 was analyzed bound to DNA, whereas the structure of Ets-1ΔN300 was determined in the absence of DNA. Importantly, the present structures show for the first time the conformation and packing of the N-terminal inhibitory helices in both the presence and absence of DNA, revealing the network of atomic contacts that are likely to participate in lowering DNA binding affinity through their effect on the ETS domain.

The most dramatic difference between the bound and unbound Ets-1 structures lies in the N-terminal inhibitory region. The N- and C-terminal inhibitory regions each contain two

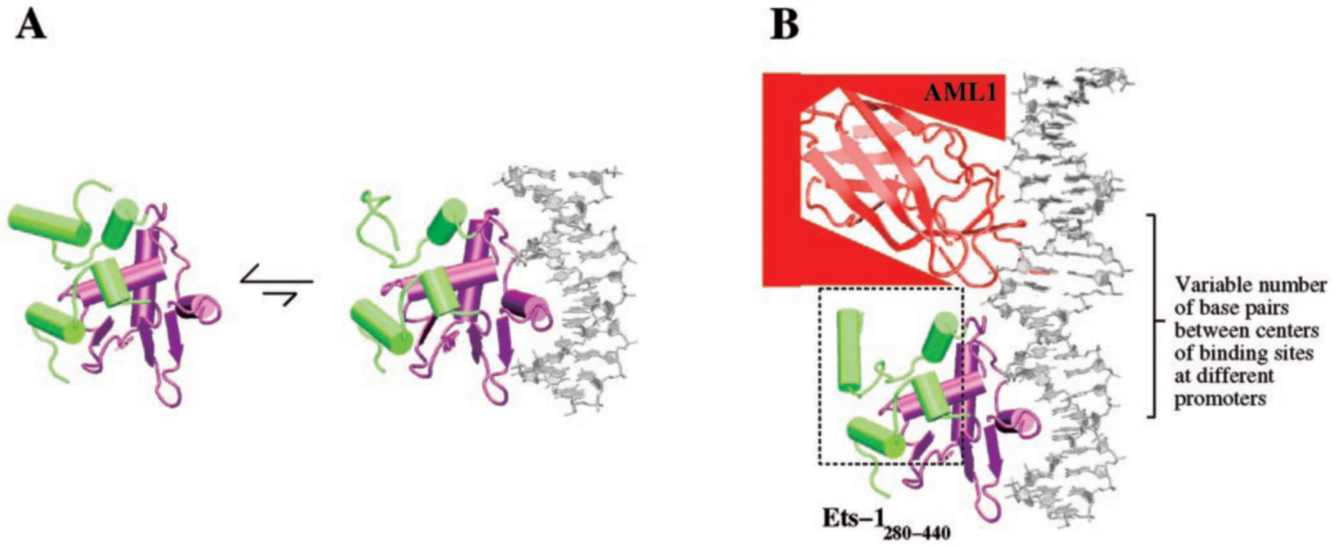

FIG. 6. **Alternative states of Ets-1ΔN280.** *A*, Ets-1ΔN280 undergoes a conformational change upon DNA binding. *B*, model of interaction between inhibitory domains of AML1, shown in *red*, and Ets-1ΔN280 on DNA. The helix HI-1 is modeled in a folded state, presumably stabilized by interactions with AML-1. Only the DNA binding domain of AML-1 is shown (35), however, additional N- and C-terminal regions, blocked in *red*, are necessary for cooperative interactions with Ets-1 (31).

α-helices: HI-1 and HI-2 in the N-terminal inhibitory region, and H4 and H5 in the C-terminal inhibitory region. The conformation of the C-terminal inhibitory helices is identical when Ets-1 is bound to DNA or free and is the same as that seen in several crystal structures of Ets-1 that lack the N-terminal inhibitory region (17) as well as in the structure of another ETS domain protein, GABPα (26). The N-terminal inhibitory helix, HI-2, makes extensive contacts with these C-terminal inhibitory helices and with helix H1 of the ETS domain (Fig. 2*C*) on a surface of the protein opposite the DNA binding (Fig. 3*C*). In the absence of DNA, an additional helix, HI-1, is found in the N-terminal inhibitory region, as predicted by solution-based studies showing that this helix is destabilized upon binding of Ets-1 to DNA. This loosely tethered helix forms reciprocal contacts with the remaining inhibitory helices and helix H1 of a neighboring monomer in the crystal, arguably mimicking the intramolecular packing of a free monomer. We have used these observed interactions to propose a model for the inhibited form of Ets-1 in the absence of DNA in which helix HI-1 packs against inhibitory helices HI-2 and H4 to form a hydrophobic core (Fig. 4). In this way, helix HI-1 serves as a critical cross brace connecting the N- and C-terminal inhibitory regions and stabilizing the inhibitory module.

Mutagenesis of the inhibited Ets-1ΔN280 supports this model and indicates that an extensive network of hydrophobic contacts stabilizes the autoinhibitory module. Mutations that alter the hydrophobic core cause constitutive disruption of the inhibitory module and reduce autoinhibition. In particular, the behavior of mutant proteins in both DNA binding and protease sensitivity studies indicates that helix HI-1 is stabilized by contacts of aromatic residues, such as Phe-304 and Tyr-307, with residues in the hydrophobic pocket formed by HI-2, H1, H4, and H5, including Tyr-424. Strikingly, these hydrophobic contacts are as crucial to the stability of the autoinhibitory module as the integrity of helix HI-1 itself. This is exemplified by the consequences of mutating of Tyr-307 in helix HI-1. Previous work demonstrated that replacement of this tyrosine with proline, which leads to unfolding of HI-1, has the same effect on autoinhibition as changing Tyr-307 to an alanine (4). In light of the structural model presented here, the stability of HI-1 and its inhibitory effect on DNA binding is linked to proper hydrophobic packing against the remainder of the Ets-1 protein.

The proposed model for the inhibited form of Ets-1 is also supported by previous mutagenesis studies. Analogous to the mutations Y307A, F304A, and Y424A reported here, Ets-1ΔN280 with alanine substitutions at either Leu-429 or Gln-339 display reduced autoinhibition due to a constitutive disruption of the inhibitory module (4, 24). The side chain of Leu-429 projects from helix H5 and is part of a hydrophobic network involving the N- and C-terminal inhibitory regions and the ETS domain. The L429A mutation would uncouple these components, leading to instability in the hydrophobic pocket and thereby disrupting the inhibitory module. Gln-339 bridges interactions between helix HI-2 and the region preceding helix H1 of the ETS domain. Disruption of this interaction by changing the charge of the side chain would destabilize the packing of HI-2 with the ETS domain thereby uncoupling the inhibitory regions from the ETS domain.

Mechanism of Autoinhibition—A key question regarding the mechanism of autoinhibition centers on how inhibitory helices that pack onto the non-DNA binding face of the protein can influence the affinity of Ets-1 for DNA. One model that has been proposed is that the packing of all four inhibitory helices against the ETS domain favors a conformation of Ets-1 that cannot form optimal contacts with the DNA (24). The reduction in DNA binding affinity of Ets-1ΔN280, as compared with Ets-1ΔN331, would therefore be due to the energetic cost of altering the structure of the inhibitory module to adopt a form suitable for binding DNA. The structures of DNA-bound and free Ets-1 presented in this study provide insights into the packing interactions that could inhibit the DNA binding of Ets-1 in this way. According to the conformational change model, helix H1 of the ETS domain plays two roles requiring two alternative conformations, one in the unbound state in which it packs with the inhibitory helices and helps stabilize the inhibitory module and another in the DNA bound state in which it contacts a DNA backbone phosphate through residues at its N terminus. Importantly, these DNA contacts involve an amide nitrogen of the peptide backbone, an interaction that may be further favored by the macrodipole of the helix. The alignment and positioning of this helix is therefore important

for optimal DNA binding (24). The model for inhibited Ets-1 derived from the Ets-1ΔN300 domain-swapped dimer structure shows the structural interconnections between the inhibitory elements and helix H1 of the ETS domain that could link the conformation of the inhibitory regions with the ability of Ets-1 to form optimal contacts with the DNA.

Although the present structures suggest a mechanism for linking the conformation and folding of the inhibitory helices with conformation of the ETS domain, a direct comparison between free Ets-1ΔN300 and Ets-1ΔN280 bound to DNA does not show a significant change in the orientation of helix H1 or other ETS domain elements. Thus, it is possible that the interactions of helix HI-1 with the opposing protein in the three-dimensional domain-swapped dimer do not exactly mimic those in the unbound inhibited monomer. Consistent with this is the modest effect of the L422A substitution on autoinhibition, even though a stronger role was predicted by our model for inhibited Ets-1 based on the domain-swapped dimer. It is therefore possible that the domain-swapped dimer represents a partially activated conformation of Ets-1. The displacement of domains or subdomains in other examples of three-dimensional domain-swapped oligomers is often accompanied by an increase in the activity of the protein. For example, in the case of $p13^{SUC1}$, the swapping of a β strand was shown to relieve packing tension in the monomer, activating the protein (27). The ability of helix HI-1 to be stabilized by a protein in *trans*, resulting in a partially activated conformation, has implications in the formation of protein partners as discussed below.

Interaction of Ets-1 with Partner Proteins—Ets-1 binds promoters in association with other DNA-binding transcription factors. Such protein partnerships have the potential to counteract autoinhibition. Results presented here and elsewhere (15, 16, 18, 24) show a strong correlation between a packed, folded helix HI-1 within the inhibitory module and reduced affinity for DNA. To bind DNA, helix HI-1 has to either unfold or perhaps be stabilized in a different orientation. Studies of the interaction of Ets-1 with other transcription factors suggest both states of helix HI-1 may be possible for the DNA-bound form of Ets-1 (Fig. 6).

The known interactions between Ets-1 and partner proteins can be divided into two categories: those that interact with the ETS domain itself (28–30) and those that interact with sequences outside the ETS domain (31, 32). For those proteins that interact with only the ETS domain, the presence of a DNA-binding partner presumably does not counteract the autoinhibition. The Ets-1/Pax-5 partnership exemplifies this type of interaction (Fig. 6*A*) (28). In the other type of interaction, direct contacts between a partner and inhibitory sequences can alleviate autoinhibition and provide cooperative energy. Helix HI-1 could be stabilized in a different conformation, allowing the ETS domain to adopt a high affinity DNA-binding form. Alternatively, the partner protein could stabilize the unfolded state of the inhibitory elements. The interaction of Ets-1 with AML1 is a potential example of this type of interaction (31, 33, 34), as AML1 binds DNA cooperatively with Ets-1ΔN280 but not Ets-1ΔN331. Mutual activation of Ets-1 and AML1 DNA binding is proposed to occur by direct interaction between their autoinhibitory domains (31, 33, 34). AML1 could contact HI-1, stabilize it, and break its intramolecular interactions, similar to that observed in the Ets-1ΔN300 crystal structure (Fig. 6*B*). This would remove the inhibitory effect of helix HI-1 on the remainder of the protein and result in high affinity DNA binding. Alternatively, the disordered residues could be stabilized, thus preventing refolding and restoration of the inhibitory module. The cooperative interaction between AML1 and Ets-1 can occur on promoters that show a varying number of base pairs between the respective DNA binding sites of AML1 and Ets-1 (31). This suggests that there is a significant degree of flexibility in the interaction between AML1 and Ets-1. The loop residues immediately following HI-1 in the linker between helices HI-1 and HI-2 do not contact the remainder of Ets-1 in the Ets-1ΔN300 structure, which suggests that they can exhibit such a degree of flexibility and allow HI-1 to adopt a number of conformations. This could contribute to the predicted flexibility in the cooperative interaction between Ets-1 and AML1.

Acknowledgment—We thank R. Campbell for help with crystallographic software.

REFERENCES

1. Johnson, P. R., Swanson, R., Rakhilina, L., and Hochstrasser, M. (1998) *Cell* **94,** 217–227
2. Karin, M., and Ben-Neriah, Y. (2000) *Annu. Rev. Immunol.* **18,** 621–663
3. Vielhaber, E. L., Duricka, D., Ullman, K. S., and Virshup, D. M. (2001) *J. Biol. Chem.* **276,** 45921–45927
4. Cowley, D. O., and Graves, B. J. (2000) *Genes Dev.* **14,** 366–376
5. Pufall, M. A., and Graves, B. J. (2002) *Annu. Rev. Cell Dev. Biol.* **18,** 421–462
6. Graves, B. J., Cowley, D. O., Goetz, T. L., Petersen, J. M., Jonsen, M. D., and Gillespie, M. E. (1998) *Cold Spring Harbor Symp. Quant. Biol.* **63,** 621–629
7. Dalton, S., and Treisman, R. (1992) *Cell* **68,** 597–612
8. Giovane, A., Pintzas, A., Maira, S. M., Sobieszczuk, P., and Wasylyk, B. (1994) *Genes Dev.* **8,** 1502–1513
9. Janknecht, R., Zinck, R., Ernst, W. H., and Nordheim, A. (1994) *Oncogene* **9,** 1273–1278
10. Lopez, M., Oettgen, P., Akbarali, Y., Dendorfer, U., and Libermann, T. A. (1994) *Mol. Cell. Biol.* **14,** 3292–3309
11. Bojovic, B. B., and Hassell, J. A. (2001) *J. Biol. Chem.* **276,** 4509–4521
12. Greenall, A., Willingham, N., Cheung, E., Boam, D. S., and Sharrocks, A. D. (2001) *J. Biol. Chem.* **276,** 16207–16215
13. Graves, B. J., and Petersen, J. M. (1998) *Adv. Cancer Res.* **75,** 1–55
14. Sharrocks, A. D. (2001) *Nat. Rev. Mol. Cell. Biol.* **2,** 827–837
15. Jonsen, M. D., Petersen, J. M., Xu, Q. P., and Graves, B. J. (1996) *Mol. Cell. Biol.* **16,** 2065–2073
16. Skalicky, J. J., Donaldson, L. W., Petersen, J. M., Graves, B. J., and McIntosh, L. P. (1996) *Protein Sci.* **5,** 296–309
17. Garvie, C. W., Hagman, J., and Wolberger, C. (2001) *Mol. Cell* **8,** 1267–1276
18. Petersen, J. M., Skalicky, J. J., Donaldson, L. W., McIntosh, L. P., Alber, T., and Graves, B. J. (1995) *Science* **269,** 1866–1869
19. Bennett, M. J., Choe, S., and Eisenberg, D. (1994) *Proc. Natl. Acad. Sci. U. S. A.* **91,** 3127–3131
20. Otwinowski, Z., and Minor, W. (1997) *Methods Enzymol.* **276,** 307–326
21. CCP4 (1994) *Acta Crystallogr. Sect. D Biol. Crystallogr.* **50,** 760–763
22. Brunger, A. T., Adams, P. D., Clore, G. M., DeLano, W. L., Gros, P., Grosse-Kunstleve, R. W., Jiang, J. S., Kuszewski, J., Nilges, M., Pannu, N. S., Read, R. J., Rice, L. M., Simonson, T., and Warren, G. L. (1998) *Acta Crystallogr. Sect. D Biol. Crystallogr.* **54,** 905–921
23. Jones, T. A., Zou, J. Y., Cowan, S. W., and M., K. (1991) *Acta Crystallogr. Sect. A* **47,** 110–119
24. Wang, H., McIntosh, L. P., and Graves, B. J. (2002) *J. Biol. Chem.* **277,** 2225–2233
25. Nye, J. A., Petersen, J. M., Gunther, C. V., Jonsen, M. D., and Graves, B. J. (1992) *Genes Dev.* **6,** 975–990
26. Batchelor, A. H., Piper, D. E., de la Brousse, F. C., McKnight, S. L., and Wolberger, C. (1998) *Science* **279,** 1037–1041
27. Schymkowitz, J. W., Rousseau, F., Wilkinson, H. R., Friedler, A., and Itzhaki, L. S. (2001) *Nat. Struct. Biol.* **8,** 888–892
28. Fitzsimmons, D., Hodsdon, W., Wheat, W., Maira, S. M., Wasylyk, B., and Hagman, J. (1996) *Genes Dev.* **10,** 2198–2211
29. Sieweke, M. H., Tekotte, H., Frampton, J., and Graf, T. (1997) *Leukemia* **11,** Suppl. 3, 486–488
30. Sieweke, M. H., Tekotte, H., Jarosch, U., and Graf, T. (1998) *EMBO J.* **17,** 1728–1739
31. Goetz, T. L., Gu, T. L., Speck, N. A., and Graves, B. J. (2000) *Mol. Cell. Biol.* **20,** 81–90
32. Bradford, A. P., Wasylyk, C., Wasylyk, B., and Gutierrez-Hartmann, A. (1997) *Mol. Cell. Biol.* **17,** 1065–1074
33. Gu, T. L., Goetz, T. L., Graves, B. J., and Speck, N. A. (2000) *Mol. Cell. Biol.* **20,** 91–103
34. Kim, W. Y., Sieweke, M., Ogawa, E., Wee, H. J., Englmeier, U., Graf, T., and Ito, Y. (1999) *EMBO J.* **18,** 1609–1620
35. Bravo, J., Li, Z., Speck, N. A., and Warren, A. J. (2001) *Nat. Struct. Biol.* **8,** 371–378